Kinetics and Mechanism of Superoxide Reduction by Two-Iron Superoxide Reductase from *Desulfovibrio vulgaris*†

Joseph P. Emerson,‡ Eric D. Coulter,‡ Diane E. Cabelli,§ Robert S. Phillips,‡ and Donald M. Kurtz, Jr.*,‡

Department of Chemistry and Center for Metalloenzyme Studies, University of Georgia, Athens, Georgia 30602, and Chemistry Department, Brookhaven National Laboratory, Upton, New York 11973

Received October 11, 2001; Revised Manuscript Received February 1, 2002

ABSTRACT: Superoxide reductases (SORs) contain a novel square pyramidal ferrous [Fe(NHis)$_4$(SCys)] site that rapidly reduces superoxide to hydrogen peroxide. Here we report extensive pulse radiolysis studies on recombinant two-iron SOR (2Fe-SOR) from *Desulfovibrio vulgaris*. The results support and elaborate on our originally proposed scheme for reaction of the [Fe(NHis)$_4$(SCys)] site with superoxide [Coulter, E. D., Emerson, J. E., Kurtz, D. M., Jr., and Cabelli, D. E. (2000) *J. Am. Chem. Soc. 122*, 11555−11556]. This scheme consists of second-order diffusion-controlled formation of an intermediate absorbing at ∼600 nm, formulated as a ferric-(hydro)peroxo species, and its decay to the carboxylate-ligated ferric [Fe(NHis)$_4$(SCys)] site with loss of hydrogen peroxide. The second-order rate constant for formation of the 600-nm intermediate is essentially pH-independent (pH 5−9.5), shows no D_2O solvent isotope effect at pH 7.7, and decreases with increasing ionic strength. These data indicate that formation of the intermediate does not involve a rate-determining protonation, and are consistent with interaction of the incoming superoxide anion with a positive charge at or near the ferrous [Fe(NHis)$_4$(SCys)] site. The rate constant for decay of the 600-nm intermediate follows the pH-dependent rate law: $k_2(\text{obs}) = k_2'[H^+] + k_2''$ and shows a significant D_2O solvent isotope effect at pH 7.7. The values of k_2' and k_2'' indicate that the 600-nm intermediate decays via diffusion-controlled protonation at acidic pHs and a first-order process involving either water or a water-exchangeable proton on the protein at basic pHs. The formation and decay rate constants for an E47A variant of 2Fe-SOR are not significantly perturbed from their wild-type values, indicating that the conserved glutamate carboxylate does not directly displace the (hydro)peroxo ligand of the intermediate at basic pHs. The kinetics of a K48A variant are consistent with participation of the lysyl side chain in directing the superoxide toward the active site and in directing the protonation pathway of the ferric-(hydro)peroxo intermediate toward release of hydrogen peroxide.

A newly emerging paradigm for protecting air-sensitive bacteria and archaea from the toxic reduction products of dioxygen involves reduction rather than disproportionation of superoxide (*1*−*4*). The reduction of superoxide via reaction 1 is catalyzed by a novel class of non-heme iron enzymes called superoxide reductases (SORs).[1]

$$e^- + O_2^- + 2H^+ \xrightarrow{\text{SOR}} H_2O_2 \qquad (1)$$

The SORs are characterized by a mononuclear active site with a ligand set consisting of a square plane of histidine nitrogens, an axial cysteine sulfur, and, in the oxidized form, a glutamate carboxylate (*5*−*7*). The SORs can be subdivided into 1Fe-SORs, which contain only the catalytic [Fe(NHis)$_4$(SCys)] site, and, 2Fe-SORs, which contain an additional [Fe(SCys)$_4$] site, whose function is presumed to be electron transfer. Among the 2Fe-SORs is the homodimeric protein originally named rubredoxin oxidoreductase (*8*) or desulfoferrodoxin (*9, 10*) from the sulfate-reducing bacterium *Desulfovibrio vulgaris*.

The X-ray crystal structure of the highly homologous 2Fe-SOR from *D. desulfuricans* revealed the unique structure of the [Fe(NHis)$_4$(SCys)] site (*6*). Subsequent X-ray crystal structures of a 1Fe-SOR from *Pyrococcus furiosus* were obtained in both the ferric and ferrous forms (*5*). These structures indicated that the functional chemistry of the [Fe(NHis)$_4$(SCys)] site in SORs must consider a redox-induced ligation/deligation of a conserved glutamate carboxylate. The ϵ-amino group of a conserved lysine residue

† This work was supported by National Institutes of Health Grant GM 40388 (D.M.K.). Pulse radiolysis studies were carried out at the Center for Radiation Chemical Research, Brookhaven National Laboratory (D.E.C.), which is supported under Contract DE-AC02-98CH10886 with the U.S. Department of Energy and supported by its Division of Chemical Sciences, Office of Basic Energy Sciences.

* To whom correspondence should be addressed. Fax: 706-542-9454. E-mail: kurtz@chem.uga.edu.

‡ University of Georgia.

§ Brookhaven National Laboratory.

[1] Abbreviations: SOR, superoxide reductase; SOD, superoxide dismutase; 1Fe-SORs, SORs that contain only the catalytic [Fe(NHis)$_4$(SCys)] site; 2Fe-SORs, SORs that contain an additional [Fe(SCys)$_4$] site; SOR$_{pink}$, 2Fe-SOR in which the [Fe(NHis)$_4$(SCys)] site is ferrous and the [Fe(SCys)$_4$] site is ferric; SOR$_{gray}$, 2Fe-SOR in which both iron sites are ferric; Tris, tris(hydroxymethyl)aminomethane; LB, Luria−Bertani medium; EDTA, ethylenediaminetetraacetic acid; MOPS, 3-(*N*-morpholino)propanesulfonic acid; IPTG, isopropyl-β-D-thiogalactoside.

10.1021/bi0119159 CCC: $22.00
Published on Web 03/06/2002

Scheme 1

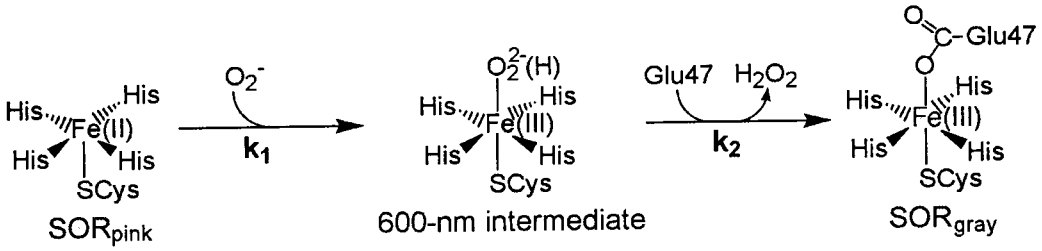

that is sequentially adjacent to the glutamate ligand approaches as closely as 6 Å to the ferrous iron in some subunits of the *P. furiosus* 1Fe-SOR structure, and this lysine side chain was, therefore, proposed as a possible electrostatic guide for superoxide into the active site (*5*).

The ferric [Fe(NHis)$_4$(SCys)] site of SORs has a broad absorption feature with a maximum at ~650 nm (ϵ_{650} ~2000 M^{-1} cm^{-1}) and a second, more intense absorption maximum at ~340 nm (*7, 10, 11*). These absorptions have been assigned to cysteinate sulfur→ferric iron charge-transfer transitions (*10, 12*). Reduction of the ferric [Fe(NHis)$_4$(SCys)] site to the ferrous form fully bleaches its visible absorption, and this bleaching provides a convenient spectroscopic probe for the redox reactivity of SORs. Due to the 100- to 200-mV more positive reduction potential of the [Fe(NHis)$_4$(SCys)] site (*10, 13*), 2Fe-SOR is typically isolated with a ferric [Fe(SCys)$_4$] site and a predominantly ferrous [Fe(NHis)$_4$(SCys)] site, even under aerobic conditions. Due to its color, this as-isolated form is referred to as SOR$_{pink}$. The diferric form of 2Fe-SOR, SOR$_{gray}$, can be prepared by oxidation of SOR$_{pink}$ using ferricyanide, hydrogen peroxide, or superoxide (*7, 10, 14*). The visible absorption spectrum of the ferric [Fe(NHis)$_4$(SCys)] site in 2Fe-SOR overlaps that of the ferric [Fe(SCys)$_4$] site, but can be readily observed in the [SOR$_{gray}$ − SOR$_{pink}$] absorption difference spectrum.

2Fe-SORs show little or no SOD activity under standard assay conditions (*1, 2, 7, 11, 15*). The ferrous [Fe(NHis)$_4$(SCys)] site of 2Fe-SOR$_{pink}$ can, nevertheless, reduce superoxide at a nearly diffusion-controlled rate (*7, 11*). Our initial mechanistic studies of the *D. vulgaris* 2Fe-SOR used pulse radiolysis of aerobic solutions to generate a bolus of superoxide in the presence of excess SOR$_{pink}$ (*7*). The subsequent buildup of visible absorption due to oxidation of the [Fe(NHis)$_4$(SCys)] site was then monitored on both microsecond and millisecond time scales. The essential results of these experiments are contained in Scheme 1. At pH 7.8 and 25 °C, the time courses of the absorbance changes at various wavelengths revealed a transient intermediate with an absorption maximum at ~600 nm (ϵ_{600} ~3500 M^{-1} cm^{-1}). This intermediate formed at a nearly diffusion-controlled rate, $k_1 \sim 1.5 \times 10^9$ M^{-1} s^{-1}, that was first order in both superoxide and SOR and decayed in a superoxide-independent but SOR-dependent first-order process with $k_2 \sim 40$ s^{-1}, to a form that was spectroscopically indistinguishable from SOR$_{gray}$. We formulated the 600-nm intermediate as a ferric-peroxo or ferric-hydroperoxo species. The E47A variant of *D. vulgaris* 2Fe-SOR, in which the ligating glutamate shown in Scheme 1 was mutated to alanine, exhibited superoxide reduction kinetics very similar to those of wild type, including the 600-nm intermediate (*7*).

Here we report a systematic and extensive investigation of the kinetics of superoxide reduction by *D. vulgaris* 2Fe-SOR and its E47A and K48A variants, the results of which allow a more complete and precise description of the mechanism shown in Scheme 1. Since our initial report, pulse radiolysis studies on other SORs have appeared (*16*−*18*), and those results are compared with ours.

MATERIALS AND METHODS

Preparation of 2Fe-SOR and Variants. Expression and purification of recombinant *D. vulgaris* 2Fe-SOR and its E47A variant have been described previously (*7*). Plasmid pK48ARbo containing the K48A-mutated *D. vulgaris* 2Fe-SOR gene was generated using pRbo as template (*7*), two complementary oligonucleotide primers containing the desired mutation (underlined): 5′-GGGGCCAAGGAAGCG-CACGTGCCGGTC-3′ and 5′-GACGGCACGTGCGCTT-CTTGGCCCC-3′, and the QuikChange mutagenesis kit (Stratagene, Inc.) following procedures described in the product manual. Oligonucleotide sequencing at the University of Georgia Molecular Genetics Instrumentation Facility confirmed the correctness of the K48A 2Fe-SOR gene sequence in pK48ARbo. This plasmid was then transformed into *E. coli* strain QC774 (*sodA*, *sod*B) for overexpression of the K48A variant (*19*). The expression and purification protocol previously described for recombinant *D. vulgaris* wild-type 2Fe-SOR (*7*) was used for the K48A variant. All 2Fe-SORs were judged to be pure by sodium dodecyl sulfate−polyacrylamide gel electrophoresis (*20*).

Metal and Protein Determinations. Metal analyses on 2Fe-SOR samples were conducted by inductively coupled plasma-atomic emission at the University of Georgia Chemical Analysis Laboratory. Protein concentrations were determined using the Bio-Rad protein assay with BSA as standard for wild-type 2Fe-SOR and wild-type 2Fe-SOR as standard for the E47A and K48A variants. 2Fe-SOR concentrations for all experiments were determined using $\epsilon_{502} = 4300$ M^{-1} cm^{-1} per monomer, which is due to the ferric [Fe(SCys)$_4$] site in SOR$_{pink}$ (*13*). Both wild-type and variant 2Fe-SORs were isolated with ferric [Fe(SCys)$_4$] and predominantly ferrous [Fe(NHis)$_4$(SCys)] sites.

SOD Assays. Using the standard assay for SOD activity (*21*), wild-type, E47A, and K48A SORs gave activities of 30, 160, and 40 units/mg, respectively. These activities may be compared with 4000 units/mg for bovine CuZn SOD and 2000 units/mg for FeSOD (*22*). Thus, the somewhat higher "SOD activity" of the E47A variant is still an order of magnitude below that of classical SODs. We have previously demonstrated by pulse radiolysis that neither the wild type nor E47A SORs possess SOD activities that could outcompete spontaneous disproportionation of micromolar levels of superoxide at pH 7.8 (*7*).

Pulse Radiolysis Experiments. The rates of reactions of *D. vulgaris* 2Fe-SOR_{pink} and its E47A and K48A variants with superoxide were measured by pulse radiolysis using the 2-MeV Van de Graaff accelerator at Brookhaven National Laboratory, as described previously (*7*). Dosimetry was calibrated using the KSCN dosimeter (*23*). Superoxide radicals were generated at radiation doses of 150−2000 rads (*24, 25*), yielding 1−20 μM superoxide per pulse in either air- or oxygen-saturated solutions containing 20−100 μM SOR_{pink} [$Fe(NHis)_4(SCys)$] sites, 10 mM sodium formate, 0.12 mM Tris, and, where stated, either 5 or 100 μM EDTA to minimize the effects of free metal ions, in water that had been purified by passage through a Millipore Ultrapurification system to achieve a resistivity of ~18 MΩ. (No significant differences in the kinetics were found for solutions containing vs omitting EDTA.) For experiments in which formate concentration was varied, formate was added from a concentrated stock solution. Ionic strength was adjusted by addition of sodium chloride. Following addition of all other reagents, the pH was adjusted by addition of either sodium hydroxide or sulfuric acid. Most studies were conducted at pH 7.7. A set of experiments was also conducted using 0.5 M ethanol in place of formate to convert OH radicals to superoxide (*26*). For solvent deuterium isotope studies, solutions were prepared identically to that described above but in 99.9 atom % D_2O (Isotek, Inc.). SOR_{pink} oxidation by superoxide was monitored at 500−700 nm via absorbance changes as a function of time from microsecond to second time scales. The sample cell path lengths were either 2 or 6.1 cm. The data were analyzed using the BNL Pulse Radiolysis Program. Except for temperature-dependent studies, all rates were measured at 25 °C. Appropriate monitoring wavelengths and concentrations of [$Fe(NHis)_4$-(SCys)] sites oxidized were determined from the absorption difference spectra of superoxide-oxidized minus as-isolated (SOR_{pink}) wild-type and variant SORs: $\epsilon_{645\ nm} = 1900\ M^{-1}\ cm^{-1}$ for wild type, $\epsilon_{580\ nm} = 1400\ M^{-1}\ cm^{-1}$ for E47A, and $\epsilon_{640\ nm} = 1600\ M^{-1}\ cm^{-1}$ for K48A SORs. The superoxide-oxidized proteins were prepared by incubation of 40−60 μM [in monomer determined using $\epsilon_{502\ nm} = 4300\ M^{-1}\ cm^{-1}$ (cf. Results)] SOR_{pink} with 0.2 mM xanthine and sufficient xanthine oxidase to generate 5−10 μM superoxide/min in 50 mM potassium phosphate, 0.1 mM EDTA, pH 7.8 (*14*). Complete oxidation of the [$Fe(NHis)_4(SCys)$] sites by the superoxide flux occurred within 5−10 min and was taken to be the point at which the visible absorbance stopped increasing.

Oxidations of 2Fe-SORs by H_2O_2. Since H_2O_2 is generated along with superoxide during pulse radiolysis (*24*), the kinetics of oxidation of the wild-type and variant ferrous [$Fe(NHis)_4(SCys)$] sites by H_2O_2 were measured. These reactions were found to be sufficiently slow so that H_2O_2 (50−2000 μM) could be manually added to SOR_{pink} solutions (50−200 μM in monomer) in a spectrophotometric cuvette, after which absorbance increases at 645 nm (wild type), 580 nm (E47A), and 640 nm (K48A) were monitored with time. Reactions were conducted aerobically at room temperature in 50 mM potassium phosphate, 0.1 mM EDTA, pH 7.8. Rates constants for oxidation of the ferrous [$Fe(NHis)_4$-(SCys)] sites were calculated from the extinction coefficients listed above for the oxidized sites. At pH 7.8 and room temperature, wild-type SOR_{pink} was oxidized to SOR_{gray} by H_2O_2 with a second-order rate constant of 21 ± 2 $M^{-1}\ s^{-1}$, which is similar to that determined for the analogous oxidation of *Da. baarsii* 2Fe-SOR (*11*). The second-order rate constants for the analogous reactions of the E47A and K48A variants were determined to be 37 ± 2 and 11 ± 1 $M^{-1}\ s^{-1}$, respectively. Some instability of the SORs was noted at the larger excesses of hydrogen peroxide. No intermediates were detected during these H_2O_2 oxidations. Given these second-order rate constants, the micromolar concentrations of H_2O_2 generated during pulse radiolysis cannot interfere with the superoxide oxidation kinetics of SOR, which occur on the microsecond to millisecond time scales.

Stopped-Flow Spectrophotometry. The kinetics of *D. vulgaris* 2Fe-SOR_{pink} oxidation by ferricyanide were monitored by stopped-flow spectrophotometry on an RSM-1000 stopped-flow spectrophotometer fitted with a rapid scanning monochromator (OLIS, Inc.). Both 2Fe-SOR and potassium ferricyanide solutions were prepared in 50 mM MOPS, pH 7.74. Solutions of 2Fe-SOR_{pink} (100 μM in [$Fe(NHis)_4$-(SCys)] sites) were mixed 1:1 (v/v) with 800 μM potassium ferricyanide in the stopped-flow instrument, and the subsequent absorbance changes at wavelengths between 440 and 680 nm were monitored.

Visible Absorption Spectrophotometry. UV/vis absorption measurements (other than stopped-flow) were measured in 1-cm path length quartz cuvettes on a Shimadzu UV2101PC scanning spectrophotometer.

RESULTS

Protein Characterization. The recombinant wild-type *D. vulgaris* 2Fe-SOR and the two variants, E47A and K48A, were each determined to contain 2.1 ± 0.3 mol of iron/mol of 2Fe-SOR monomer. These values indicated full occupancy of both [$Fe(SCys)_4$] and [$Fe(NHis)_4(SCys)$] sites by iron in all three proteins. Zinc and other transition-metal contents were negligible (<0.05 mol of metal/mol of monomer) for all three 2Fe-SORs. These metal analyses in combination with the BioRad protein assay (using wild-type 2Fe-SOR as a standard) yielded a molar extinction coefficient of 4.2 $mM^{-1}\ cm^{-1}$/monomer at 502 nm for both E47A and K48A variants, which is identical within experimental error to the published value of 4.3 $mM^{-1}\ cm^{-1}$ for the wild-type protein (*13*). We also verified by gel filtration that all three 2Fe-SORs are dimeric at the protein concentrations used in this study (*27*). Throughout the Results section, these three *D. vulgaris* 2Fe-SORs are referred to simply as either wild-type or variant SORs.

Wild-Type SOR: Pulse Radiolysis Kinetics. Figure 1A,B depicts representative 600-nm absorbance vs time traces for reactions of wild-type SOR_{pink} with superoxide generated by pulse radiolysis at pH 7.7 and 25 °C. These experiments were conducted under pseudo-first-order conditions in which the concentration of [$Fe(NHis)_4(SCys)$] sites (20−100 μM) was typically in 5−100-fold molar excess over the superoxide generated by each pulse. Verifying our previous results, the rate of formation of the 600-nm absorbing intermediate was found to be first order in both superoxide (1−5 μM O_2^-) and SOR (between 20 and 100 μM [$Fe(NHis)_4(SCys)$] sites), whereas the rate of decay of this intermediate was found to

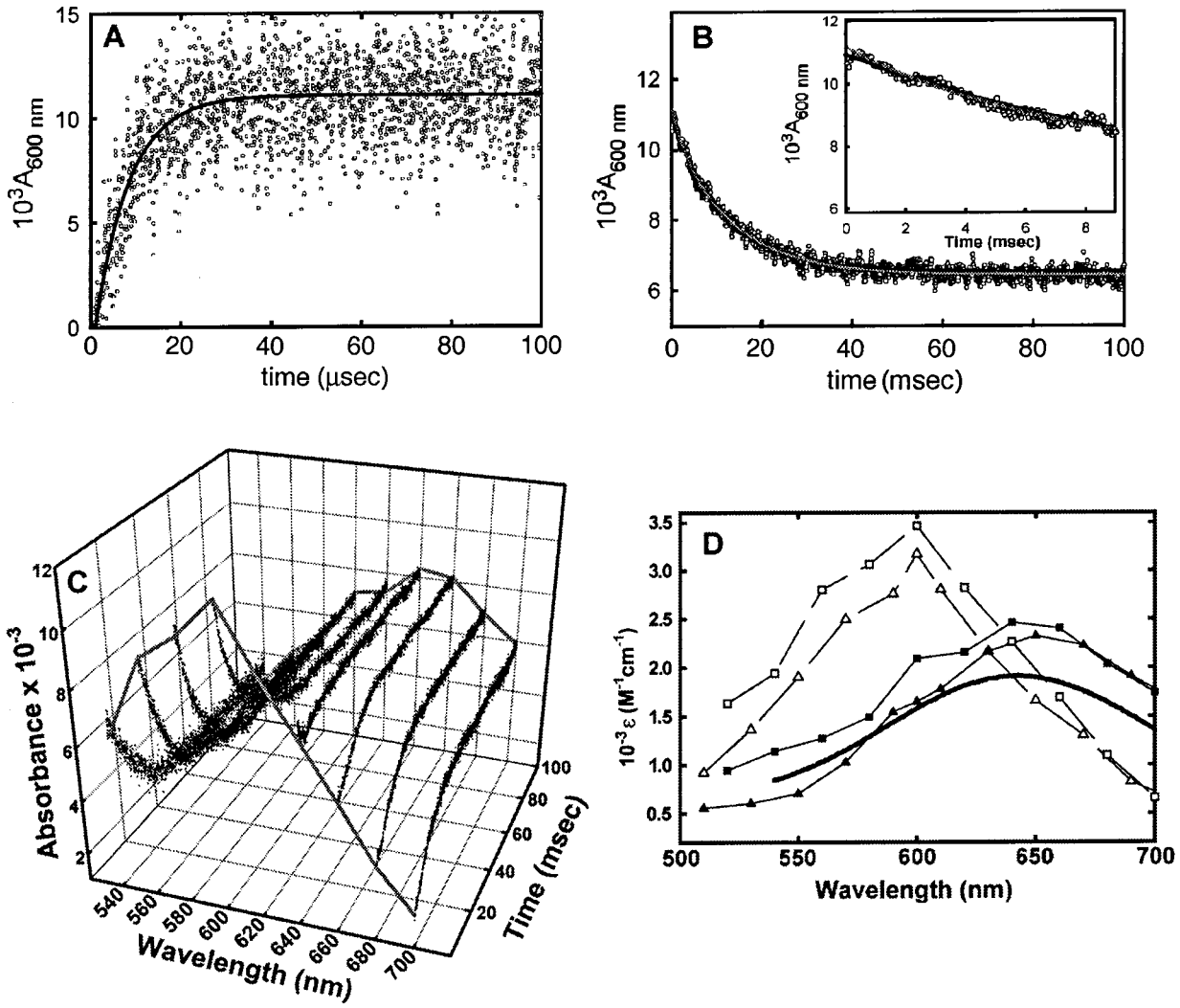

FIGURE 1: Absorbance vs time courses at 25 °C for formation (A) and decay (B and C) of the 600-nm intermediate following pulse radiolysis of 100 μM wild-type SOR_{pink} [$Fe(NHis)_4(SCys)$] sites with 1.7 μM O_2^-. In panel B, both one exponential (black curve) and sum of two exponential fits (gray curve) using the values listed in the text and tables are shown as solid curves through the data points. Panel D shows spectra of the intermediate (open symbols) 75 μs and product (closed symbols) 100 ms after the superoxide pulse constructed from molar absorptivities of kinetic traces from reactions of wild-type SOR_{pink} (25−100 μM in [$Fe(NHis)_4(SCys)$] sites) with 1.1−1.7 μM O_2^-. Molar absorptivities were calculated assuming a quantitative 1:1 mol/mol reaction of superoxide with ferrous [$Fe(NHis)_4(SCys)$] sites. All solutions were aerobic in 0.12 mM Tris and 10 mM formate, pH 7.8. Solutions in panels A and B also contained 5 μM EDTA. The spectra in panel D are plotted for reactions at both pH 7.8 (squares) and pH 5.5 (triangles). The "resting" absorption difference spectrum of [SOR_{gray} − SOR_{pink}] (smooth thick curve) at pH 7.8 is included for comparison.

Table 1: Rate Constants for Formation, k_1, and Decay, k_2, of the Intermediate during Reaction of *D. vulgaris* Wild-Type and Variant 2Fe-SOR [$Fe^{II}(NHis)_4(SCys)$] Sites with Superoxide, As Measured by Pulse Radiolysis[a]

SOR	$10^{-9}k_1$ ($M^{-1}s^{-1}$)	k_2 (s^{-1})
wild type	1.4 (±0.3)	84 (±2)
E47A	2.2 (±0.3)	65 (±6)
K48A	0.21 (±0.01)	25 (±10)

[a] Rates were determined from the time courses of absorbance changes at 600 nm following pulse radiolysis at 25 °C in solutions containing 100 μM SOR_{pink} [$Fe(NHis)_4(SCys)$] sites, 0.12 mM Tris, 5 μM EDTA, 10 mM formate, pH 7.7, and pulsed with 1.1−1.7 μM O_2^-. Ranges listed in parentheses are the averages of 3−5 determinations.

be independent of superoxide concentration. Table 1 lists the rate constants derived from fits of these and analogous time courses assuming that single exponential functions accurately describe the absorbance vs time courses for both a second-order formation and first-order decay of the 600-nm intermediate. Because pulse radiolysis studies on other SORs have indicated formation of a second distinct chromophoric intermediate maximizing ~5 ms following the superoxide pulse (*16*, *17*), we closely examined our decay curves for such a chromophore. Figure 1B shows that a sum of two exponential functions with $k_2 = 350\ s^{-1}$ and $k_3 = 80\ s^{-1}$ (gray curve) visually appears to provide a marginally improved fit of the time course for decay of the 600-nm intermediate. The sum-of-two exponentials fit would imply a second transient, i.e., a reaction sequence such as in eq 2:

$$SOR_{pink} + O_2^- \xrightarrow{k_1} \text{600-nm intermediate} \xrightarrow{k_2} {}^{2nd}\text{-intermediate} \xrightarrow{k_3} SOR_{gray} + H_2O_2 \quad (2)$$

However, the calculated goodness-of-fit parameters indicated that the sum-of-two-exponentials did not constitute a significant improvement over a one-exponential fit with $k_{obs} = 80\ s^{-1}$ (black curve). Furthermore, the family of kinetic

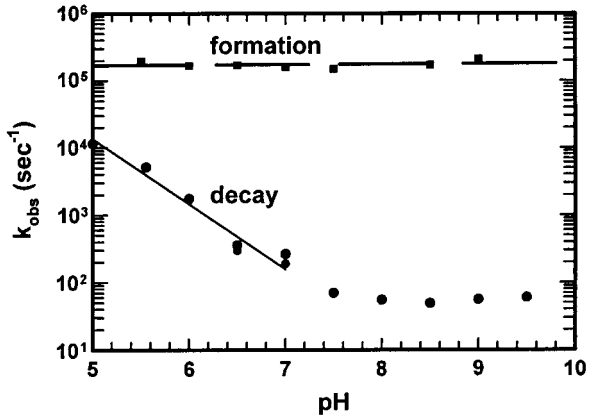

FIGURE 2: pH dependence of the formation and decay rate constants of the 600-nm intermediate in the pulse radiolysis reaction of wild-type SOR_{pink} with O_2^-. Kinetics data were collected 25 °C from A_{600} vs time traces following pulse radiolysis to generate 1.6−2.0 μM superoxide in solutions containing 100 μM (in [Fe(NHis)$_4$(SCys)] sites) SOR_{pink} in aerobic 10 mM formate, 0.12 mM Tris.

transients plotted in Figure 1C and the absorption spectra constructed therefrom in Figure 1D show no evidence for distinct chromophores other than those of the initial 600-nm intermediate and final product.

The extinction coefficients for the intermediate and final product of pulse radiolysis on the *y*-axis of Figure 1D were calculated assuming that each superoxide generated during a pulse oxidizes one [Fe(NHis)$_4$(SCys)] site in SOR_{pink}. The reasonably good agreement of the product spectrum in Figure 1D obtained 100 ms following the superoxide pulse with the "resting" SOR_{gray} spectrum, using the criteria of extinction coefficient [ϵ_{647} = 1900 M^{-1} cm^{-1} (*7*)], λ_{max}, and overall shape of the absorption curve confirms the one-electron nature of the reaction. This determination also means that the pulse radiolysis kinetics do not represent the sum of reaction rates of superoxide with the ferrous sites plus a portion of the newly formed ferric sites, as could in principle occur for SOD-type chemistry. Our pulse radiolysis kinetics are, thus, adequately described by formation of a single 600-nm absorbing intermediate on the 100-μs time scale and its decay to the "resting" SOR_{gray} state on the 100-ms time scale.

As expected for a rate constant exceeding 10^9 M^{-1} s^{-1}, the rate of formation of the 600-nm intermediate was found to be only modestly temperature-dependent, showing an approximate 2.5-fold increase between 15 and 75 °C. From the Erying plot (cf. Supporting Information), the activation parameters for formation of the 600-nm intermediate were estimated to be $\Delta H^{\ddagger}_{formation}$ = +2 kcal/mol, $\Delta S^{\ddagger}_{formation}$ = −24 cal/(mol·K), and $\Delta G^{\ddagger}_{formation}$ = +11 kcal/mol. These values are reasonable for a second-order associative mechanism involving diffusion of a small molecule to an open coordination site in a metalloprotein (*28*, *29*). The rate constant for decay of the 600-nm intermediate appeared to exhibit a much larger temperature dependence, increasing approximately 80-fold between 15 and 75 °C, with the following activation parameters: $\Delta H^{\ddagger}_{formation}$ = +12 kcal/mol, $\Delta S^{\ddagger}_{formation}$ = −2 cal/(mol·K), and $\Delta G^{\ddagger}_{formation}$ = +14 kcal/mol. Unfortunately, the pK_a of Tris, which was used to buffer these solutions, decreases significantly with increasing temperature (∼−0.03 ΔpK_a/°C) (*30*). Since, as shown below, the decay rate constant, k_2, increases significantly at acidic pHs, the temperature dependence of k_2 is likely to be convoluted with its pH dependence in Tris buffer.

Table 2: Temperature, pH, and Ionic Strength Dependences of the Rate Constants for Formation, k_1, and Decay, k_2, of the Intermediate during Reaction of *D. vulgaris* 2Fe-SOR [Fe^{II}(NHis)$_4$(SCys)] Sites with Superoxide, As Measured by Pulse Radiolysis[a]

T (°C)	$10^{-9}k_1$ (M^{-1} s^{-1})	k_2 (s^{-1})
15.5	1.0 (±0.2)	62 (±2)
25.0	1.1 (±0.1)	79 (±6)
34.2	1.5 (±0.1)	140 (±2)
44.2	1.6 (±0.1)	370 (±20)
53.9	2.1 (±0.1)	750 (±50)
59.4	2.4 (±0.1)	1140 (±80)
75.0	2.6 (±0.3)	4800 (±540)
pH	$10^{-9}k_1$ (M^{-1} s^{-1})	k_2 (s^{-1})
5.5	2.0 (±0.1)	5400 (±300)
6.0	1.7 (±0.2)	1700 (±200)
6.5	1.7 (±0.1)	330 (±20)
7.0	1.6 (±0.1)	270 (±45)
7.5	1.5 (±0.3)	72 (±5)
8.0	1.5 (±0.2)	55 (±4)
8.5	1.7 (±0.1)	49 (±3)
9.0	1.7 (±0.3)	56 (±1)
9.5	ND[b]	60 (± 4)
NaCl (mM)	$10^{-9}k_1$ (M^{-1} s^{-1})	k_2 (s^{-1})
0	1.1 (±0.2)	96 (±3)
31	0.75 (±0.1)	92 (±4)
62	0.66 (±0.04)	94 (±3)
125	0.53 (±0.02)	93 (±4)
250	0.34 (±0.03)	84 (±3)
400	0.26 (±0.05)	66 (±3)

[a] Rates were determined from the time courses of absorbance changes at 600 nm following pulse radiolysis, as described under Materials and Methods. Unless otherwise indicated, all reactions were carried out at 25 °C in solutions containing 100 μM SOR_{pink} [Fe(NHis)$_4$(SCys)] sites, 0.12 mM Tris, 5 μM EDTA, 10 mM formate, pH 7.7, and pulsed with 1.1−1.7 μM O_2^-. Ranges listed in parentheses are the averages of 3−5 determinations. [b] Not determined.

The pH dependences for rates of formation and decay of the 600-nm intermediate are plotted in Figure 2 from the data listed in Table 2. The rate constant for formation of the 600-nm intermediate is nearly invariant over the pH range 5−9.5, indicating the lack of involvement of either protons or hydroxide in the rate-determining step. The pH independence of the absorption spectrum of the intermediate in Figure 1D further supports this interpretation. The pH/rate profile for the decay contains an "upward bend" below pH 7.5, which is typically analyzed in terms of separate pathways consisting of rate-determining protonation at low pH and either attack by water or unimolecular decomposition at high pH. The observed pH dependence of the decay can, thus, be analyzed according to $k_2 = k_2'[H^+] + k_2''$, where k_2' applies to a second-order protonation of the 600-nm intermediate and k_2'' applies to a first-order pH-independent decay of this intermediate. From a fit of this equation to the data plotted in Figure 2, k_2' is estimated to be 1.5 × 10^9 M^{-1} s^{-1}, and k_2'' is estimated to be 50 s^{-1}. This analysis, thus, suggests that the biphasic pH dependence arises from rapid (approaching diffusion-controlled) protonation of the 600-nm intermediate at low pH that is outcompeted at high pH by a first-order pH-independent decay process.

Figure 3 plots the ionic strength dependences of the formation and decay rate constants for the 600-nm intermediate, and the corresponding data are listed in Table 2. At

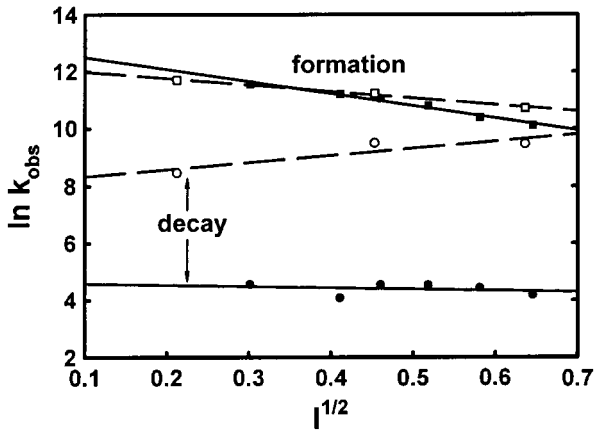

FIGURE 3: Ionic strength dependences of formation (squares) and decay (circles) rate constants for the 600-nm intermediate in the pulse radiolysis reaction of wild-type SOR_{pink} with superoxide according to Scheme 1 (cf. text). Closed symbols are at pH 7.7, and open symbols are at pH 5.5. Data were collected under the conditions listed in the Figure 2 legend except that the solutions contained 5 μM EDTA. Ionic strength was adjusted by addition of NaCl.

pH 7.7, the 600-nm intermediate shows an approximate 4-fold decrease in its rate of formation as ionic strength increases over 0−0.4 M NaCl (0.1−0.7 $\mu^{1/2}$, including the 0.01 M formate),[2] whereas the corresponding decay rate decreases by no more than 1.3-fold over the same ionic strength range. At pH 5.5, the formation rate constant, k_1, shows essentially the same ionic strength dependence as at pH 7.7, as expected if proton transfer is not rate-determining (the pK_a of H_2O, 4.8, would not be a significant factor in the pH range examined here). The decay constant, k_2, however, shows a definite increase with increasing ionic strength at pH 5.5, as opposed to the relative invariance seen at pH 7.7. The ~5-fold increase in k_2 from 0 to 0.4 M NaCl at pH 5.5 is consistent with the decay consisting of rate-determining protonation of a positively charged intermediate by solvent at this acidic pH.

Consistent with the ionic strength and pH dependences, the decay, but not the formation, rate constant shows a substantial solvent D_2O effect. For two consecutive sets of pulse radiolysis experiments carried out at pH 7.7 and 25 °C in H_2O and D_2O, respectively, under otherwise identical conditions, $k_1[H_2O]/k_1[D_2O] = 1.2(\pm 0.3)$, whereas $k_2[H_2O]/k_2[D_2O] = 60\ (\pm 2)/30(\pm 2) = 2.0(\pm 0.2)$. Thus, a proton transfer in the rate-determining step is evident in decay but not in formation of the 600-nm intermediate at pH 7.7.

Wild-Type SOR: Oxidation by Ferricyanide. To compare the kinetics of SOR_{pink} oxidation by superoxide with other one-electron oxidants, we examined the oxidation of SOR_{pink} with ferricyanide by stopped-flow spectrophotometry. Absorbance increases were monitored at fixed wavelengths of 600 and 650 nm and also by rapid scanning spectrophotometry between 440 and 680 nm up to 2 s following stopped-flow mixing. At 25 °C in 50 mM MOPS, pH 7.4, 50 μM $[Fe(NHis)_4(SCys)]$ site of SOR_{pink} was oxidized by 400 μM potassium ferricyanide to a species indistinguishable from SOR_{gray} with a rate constant of 30 ± 0.3 s^{-1}, as determined from $\Delta A_{650\ nm}$ vs time data (cf. Supporting Information). No faster forming intermediate with absorption in the range of 440−680 nm was detected to have accumulated prior to the mixing dead time (~2 ms). Fitting of the $\Delta A_{650\ nm}$ time courses with a sum of two exponentials did not improve the fit over the single 30-s^{-1} exponential.

E47A and K48A SOR Pulse Radiolysis Kinetics. The data presented in Figure 4 and Table 1 indicate that the intermediate formed upon pulse radiolysis of the E47A SOR_{pink} variant has kinetics and absorption spectral characteristics closely resembling those of the wild type at pH 7.8, i.e., second-order, nearly diffusion-controlled formation of a 600-nm absorbing intermediate on the 100-μs time scale and its first-order, single-exponential decay on the 100-ms time scale. The decay time course for E47A SOR in Figure 4B was also fit to a sum of two exponentials according to reaction sequence 2 with $k_2 = 350\ s^{-1}$ and $k_3 = 70\ s^{-1}$. As for wild-type SOR, while visually appearing to provide a slightly better fit to the early stages of the E47A decay curve, the sum-of-two-exponentials did not constitute a statistically significant improvement over the one-exponential fit with $k_2 = 65\ s^{-1}$, and the 3-dimensional plot in Figure 4C shows no evidence for a second distinct chromophore between the 600-nm intermediate and final product. The final product spectrum, constructed from data obtained at 100 ms (Figure 4D), is once again in reasonably good agreement with the "resting" E47A SOR_{gray} absorption spectrum at pH 7.8 (*7*). Removal of the E47 carboxylate ligand could in principle allow solvent coordination to the $[Fe(NHis)_4(SCys)]$ site. The absorption spectrum of the E47A intermediate (cf. Figure 4D), however, closely resembles that of the wild type (compare Figure 1D), and is essentially pH-independent between 5.6 and 9.1. These results show that the E47 carboxylate does not affect either the rate of formation or the nature of the intermediate, nor does it affect its decay at pH 7.8.

The first detectable intermediate upon pulse radiolysis of K48A SOR_{pink} forms with a second-order rate constant (cf. Table 1 and Figure 5A) that is 6−7-times slower than that for formation of the wild-type intermediate under the same conditions (pH 7.7). The ionic strength dependence of the K48A formation rate constant is also much smaller than for wild type (cf. Supporting Information). The first-order decay of the K48A intermediate was 3−4-fold slower than for wild type under the same conditions (cf. Table 1 and Figure 5B,C). The initial portion of the K48A decay trace in Figure 5B shows evidence of a second intermediate, i.e., that the reaction 2 sequence may apply. Fits of this decay curve with a sum of two exponentials yielded $k_2 = 275\ s^{-1}$ and $k_3 = 20\ s^{-1}$. However, once again, the family of decay transients in the 3-D plot of Figure 5C showed no clear evidence for a distinct chromophore that could be associated with a second intermediate (which for $k_2 = 275\ s^{-1}$ should accumulate maximally at ~8 ms reaction time). Furthermore, the absorption spectrum of the K48A intermediate obtained 800 μs after pulse radiolysis (Figure 5D) is very similar to that

[2] The formation and decay rate constants were found to be only modestly dependent on the concentration of formate (cf. Supporting Information), which was used to convert hydroxyl radicals to superoxide in the pulse radiolysis solutions (*23*). Spectroscopic monitoring indicated that formate does not form a complex with the ferric $[Fe(NHis)_4(SCys)]$ site of SOR_{gray} in the concentration range used for the pulse radiolysis. The same 600-nm intermediate was found to form in pulse radiolysis experiments using 0.5 M ethanol rather than formate to generate superoxide (cf. Supporting Information).

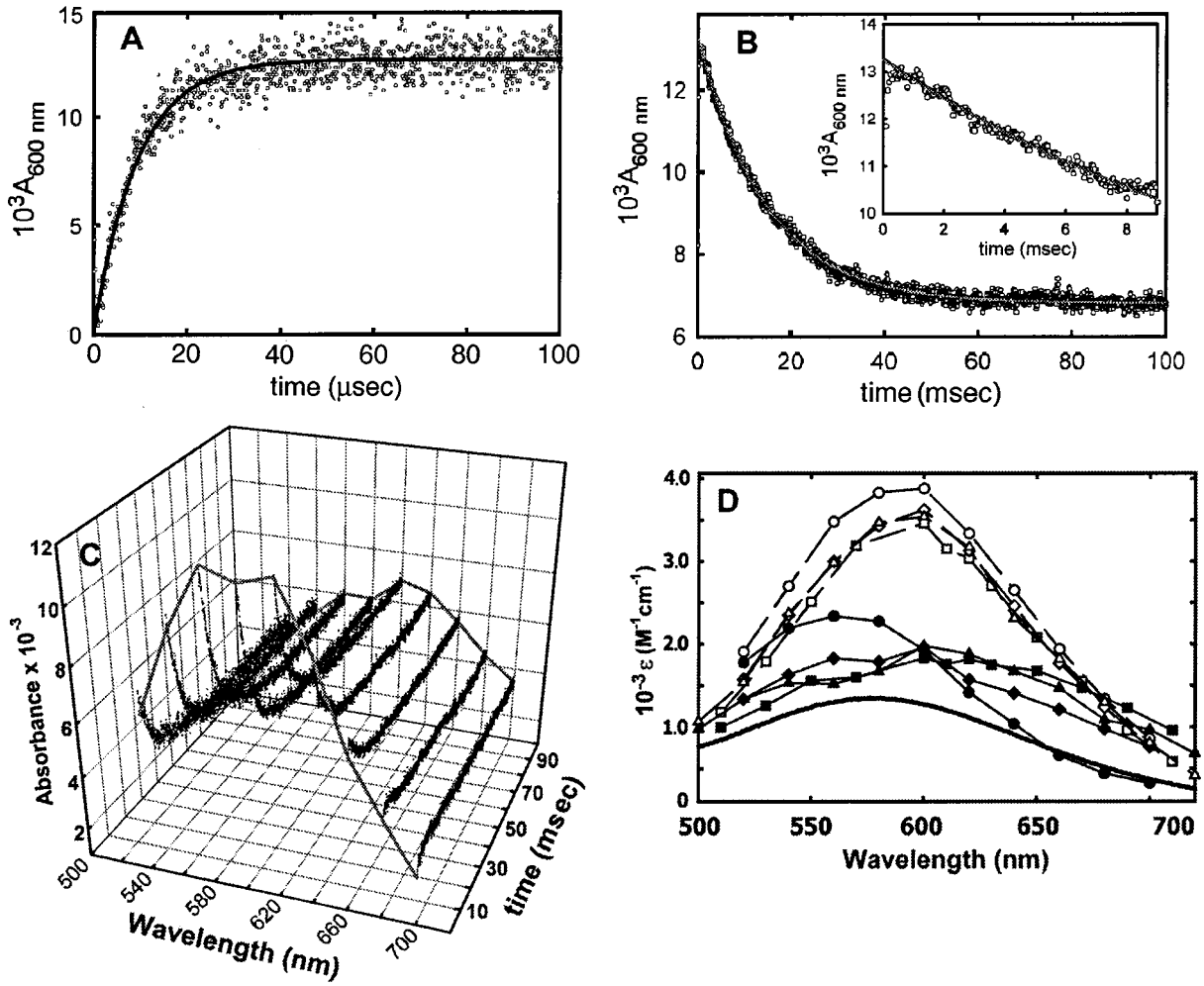

FIGURE 4: Absorbance vs time courses at 25 °C for formation (A) and decay (B and C) of the 600-nm intermediate following pulse radiolysis of 50−100 μM E47A SOR_{pink} [$Fe(NHis)_4(SCys)$] sites with 1.7 μM O_2^-. In panel B, both one exponential (black curve) and sum of two exponential fits (gray curve) using the values listed in the text and tables are shown as solid curves through the data points. Panel D plots spectra of the E47A intermediate (open symbols) 75 μs and product (closed symbols) 100 ms after the superoxide pulse constructed from molar absorptivities calculated as described in the Figure 1 legend. All solutions were aerobic in 0.12 mM Tris and 10 mM formate, pH 7.8, with 5 μM (panels A and B) or 100 μM (panel D) EDTA added. Spectra in panel D are plotted at pH 9.1 (circles), 7.8 (diamonds), 6.7 (triangles), and 5.6 (squares). The "resting" absorption difference spectrum of E47A [SOR_{gray} − SOR_{pink}] (smooth thick curve) at pH 7.8 is included for comparison.

of wild type, with an absorption maximum at ~590 nm (ϵ_{590} ~ 3600 M^{-1} cm^{-1}).

DISCUSSION

Scheme 2 is a refinement of Scheme 1 that follows directly from the results presented here. The key evidence for Scheme 2 can be summarized as follows:

(i) The oxidation kinetics of the ferrous [$Fe(NHis)_4(SCys)$] site in *D. vulgaris* SOR_{pink} by superoxide consist of second-order formation of an intermediate absorbing at 600 nm and its first-order decay to a species indistinguishable from the ferric, carboxylate-ligated site of SOR_{gray}.

(ii) The lack of any detectable intermediate during oxidation of the ferrous [$Fe(NHis)_4(SCys)$] site by the outer-sphere oxidant ferricyanide, despite the very similar overall time scales for oxidation by ferricyanide and superoxide, further supports the chemically reasonable formulation of the 600-nm intermediate as the product of an inner-sphere redox reaction of superoxide with the ferrous [$Fe(NHis)_4(SCys)$] site, generating a ferric-(hydro)peroxo species.

(iii) The second-order rate constant exceeding 10^9 M^{-1} s^{-1}, the low positive activation enthalpy, and the negative activation entropy for formation of the 600-nm intermediate are all consistent with rate-determining diffusion of superoxide to the ferrous [$Fe(NHis)_4(SCys)$] site.

(iv) The formation rate constant for the 600-nm intermediate decreases with increasing ionic strength, consistent with interaction of the incoming superoxide anion with a positive charge at or near the ferrous [$Fe(NHis)_4(SCys)$] site.

(v) The rate constant for formation of the 600-nm intermediate is essentially pH-independent (pH 5−9.5) and shows no D_2O solvent isotope effect; i.e., its formation does not involve a rate-determining protonation.

(vi) The first-order rate constant for decay of the 600-nm intermediate follows the pH-dependent rate law: $k_2(obs) = k_2'[H^+] + k_2''$, and shows a significant D_2O solvent isotope effect at pH 7.7. The values of k_2' and k_2'' indicate that the 600-nm intermediate converts to SOR_{gray} via a diffusion-controlled protonation by either solvent or a protein residue at acidic pHs and a pH-independent first-order process

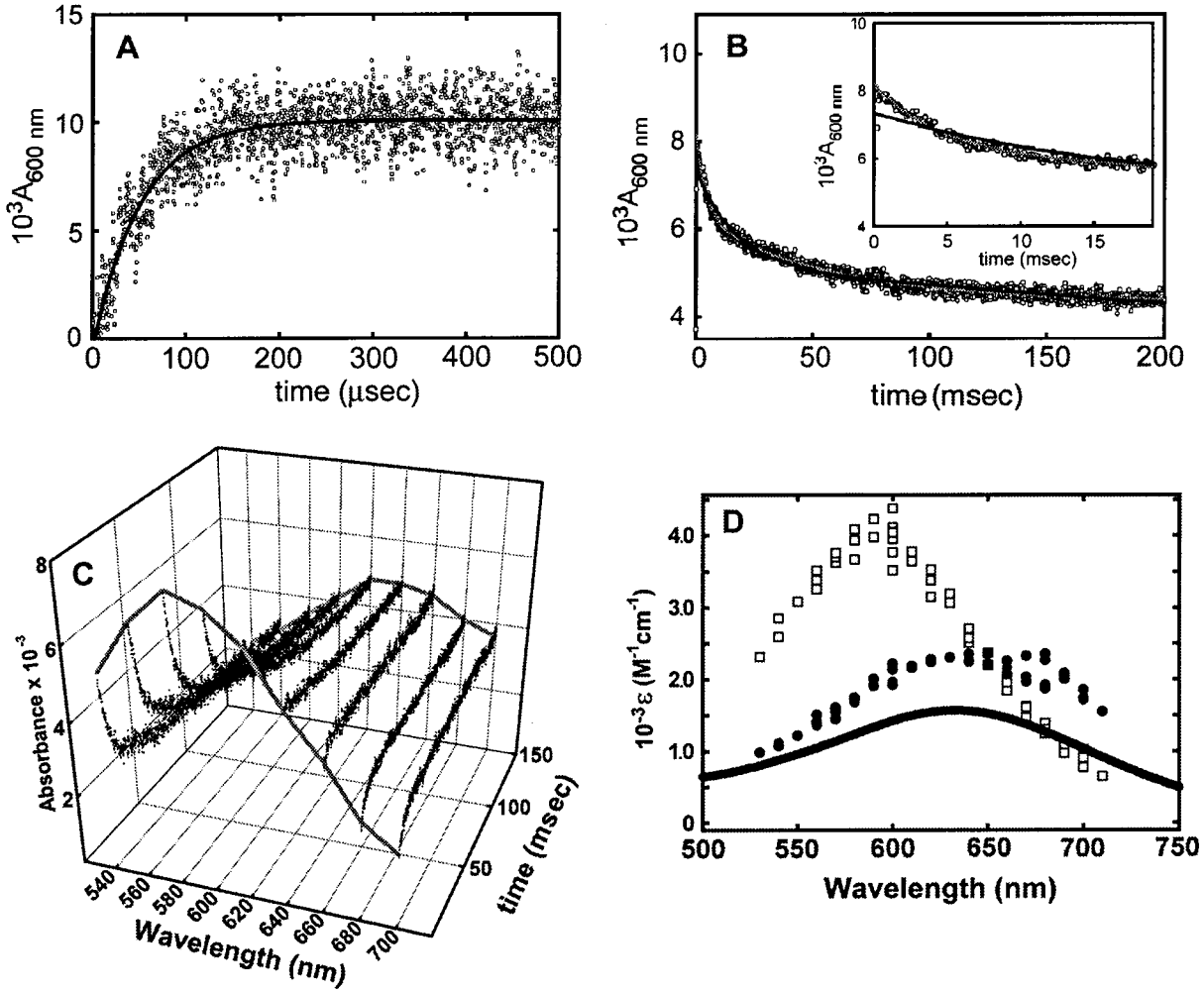

FIGURE 5: Absorbance vs time courses at 25 °C for formation (A) and decay (B and C) of the 600-nm intermediate following pulse radiolysis of 100 μM K48A SOR_{pink} [$Fe(NHis)_4(SCys)$] sites with 1.2 μM (panels A and B) or 1.0 μM (panel C) O_2^-. In panel B, both one exponential (black curve) and sum of two exponential fits (gray curve) using the values listed in the text and tables are shown as solid curves through the data points. Panel D plots spectra of the intermediate (open squares) 300 μs and final product (closed circles) 200 ms after the superoxide pulse for reactions of K48A SOR_{pink} (100 μM in [$Fe(NHis)_4(SCys)$] sites) with 1.3−1.7 μM O_2^- at 25 °C. Molar absorptivities were calculated as described in the Figure 1 legend. Spectra constructed from three sets of experiments are plotted. All solutions were aerobic in 0.12 mM Tris and 10 mM formate, pH 7.8. The "resting" absorption difference spectrum of K48A [SOR_{gray} − SOR_{pink}] (smooth thick curve) at pH 7.8 is included for comparison.

involving water or a water-exchangeable proton on the protein at basic pHs.

(vii) The rate constant for decay of the 600-nm intermediate increases with increasing ionic strength at pH 5.5, which, together with the rate law in (vi), suggests diffusion-controlled protonation of a positively charged intermediate at acidic pHs.

Assuming that the coordination sphere of the ferrous [$Fe(NHis)_4(SCys)$] site is retained, a ferric-peroxo adduct would be overall charge-neutral (i.e., four neutral imidazolyls, cysteinate and peroxo ligated to Fe^{III}). Based on the structures of other SORs (*5*, *6*), the conserved Lys48-ϵNH_3^+ in *D. vulgaris* 2Fe-SOR appears to be the only positively charged center near the [$Fe(NHis)_4(SCys)$] site at neutral pH, and to be localized above what would be the peroxo coordination position. The Lys48-ϵNH_3^+ would, therefore, likely be attracted to the negatively charged peroxo ligand. The absorption spectra in Figures 1D and 4D show that the 600-nm intermediate does not have a pK_a between pH 5.6 and 9.1. The apparently diffusion-controlled acid-catalyzed decay pathway in Scheme 2 that dominates at acidic pHs could then consist of disruption of the Lys48-$\epsilon NH_3^+ \cdots O_2^{2-}$ salt bridge by protonation of the ferric-peroxo followed by rapid addition of a second proton and release of H_2O_2. The pH-independent, first-order decay pathway in Scheme 2, which dominates at basic pHs, could involve rate-determining water attack on the ferric-peroxo or, as formulated in Scheme 2, proton transfer from the lysyl side chain to a peroxo oxygen. Either explanation is consistent with the solvent D_2O effect on k_2 at pH 7.7.

Our data do not rule out an alternative mechanism consisting of rapid protonation of an initially formed ferric-peroxo to generate a ferric-hydroperoxo 600-nm intermediate. If so, however, the rate constant for this rapid protonation of the ferric-peroxo would have to exceed 10^{10} M^{-1} s^{-1} in order to explain the pH and D_2O independence of a formation rate constant exceeding 10^9 M^{-1} s^{-1}. A protein side chain might conceivably supply a proton sufficiently rapidly to form a ferric-hydroperoxo 600-nm intermediate. However, the only proximal side chain capable of proton donation at pH 7.8 appears to be the ϵ-amino group of K48, and the K48A variant forms a spectrally nearly identical 600-nm

Scheme 2

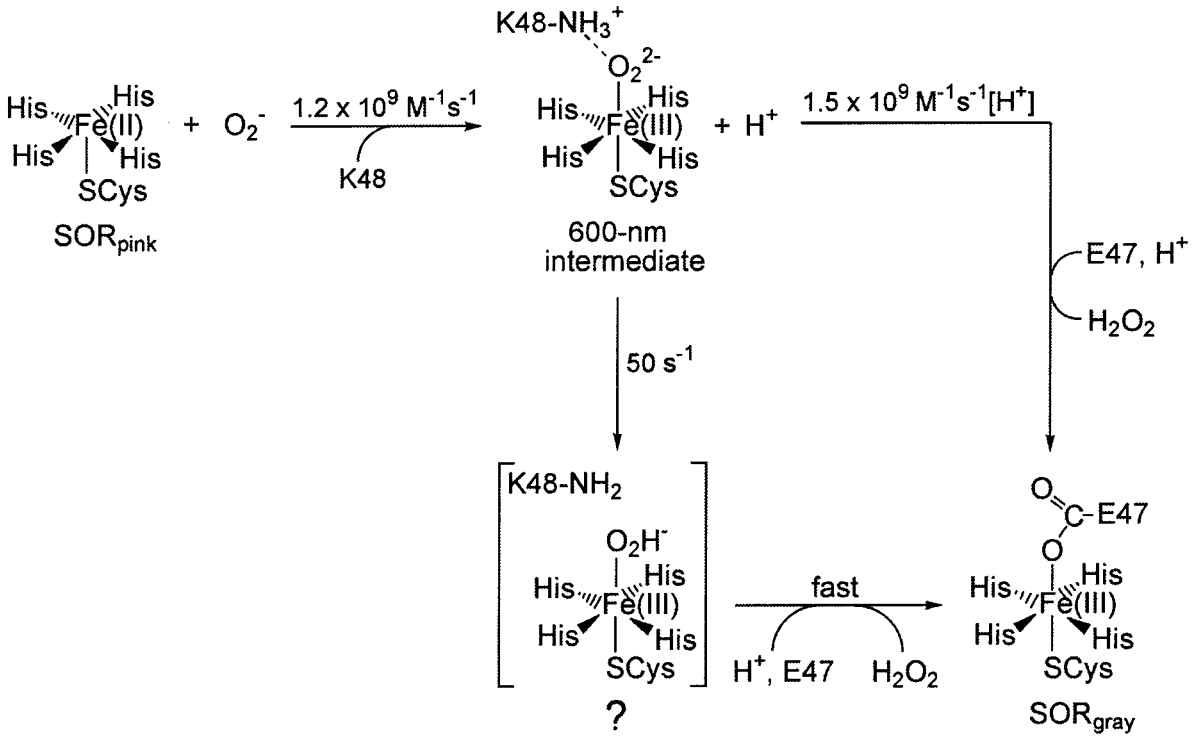

intermediate, albeit 6−7-times slower than does wild type. A ferric-hydroperoxo 600-nm intermediate in the K48A variant would presumably have to acquire its proton directly from solvent.

The same 600-nm intermediate forms in the E47A variant (compare Figure 4D with Figure 1D). The lack of significant perturbation of the formation and decay rate constants from their wild-type values in the E47A variant (cf. Table 1) suggests that Glu47 enters after the rate-determining step during decay of the 600-nm intermediate above pH 7, i.e., that the carboxylate of Glu47 does not directly displace the (hydro)peroxo ligand of the 600-nm intermediate at basic pHs. Since we did not detect any other distinct species between the 600-nm intermediate and final product, we can only infer the existence of a transient species, which is formulated as a hydroperoxo adduct within brackets in Scheme 2. At pH 5.5, on the other hand, k_2 for the E47A variant is significantly lower than for wild type (data not shown) even though, like the wild type, the E47A intermediate does not have a pK_a near pH 5.5 (cf. Figure 4D). These results are consistent with some involvement of E47 in decay of the 600-nm intermediate at acidic pHs. The minimal involvement in superoxide reduction kinetics at or above neutral pH of this strictly conserved glutamate, a result also reported for a 1Fe-SOR (*18*), is somewhat surprising. One possible explanation is that in vivo this glutamate prevents coordination of small molecules to the "resting" ferric [Fe(NHis)$_4$(SCys)] site that would either inhibit SOR activity or result in adventitious side reactions, but that, during SOR turnover, this glutamate does not ligate iron.

The fairly modest effect of K48A substitution on the decay kinetics (3−4-fold slower with much smaller ionic strength dependence and some evidence for a second intermediate) may underemphasize an important role for K48. In addition to its proposed role in directing or orienting superoxide for reaction with the ferrous [Fe(NHis)$_4$(SCys)] site (consistent with the lowered ionic strength effect on formation of the K48A intermediate), the interaction with K48 shown in Scheme 2 may affect how the ferric-peroxo intermediate is protonated during its decay. If the intermediate contains an end-on-coordinated peroxo, protonation of the iron-bound oxygen atom is likely to favor dissociation as hydrogen peroxide, whereas protonation of the terminal oxygen would more likely favor O−O bond cleavage. These alternative proton-directed decay pathways have, in fact, been proposed to occur in the structurally analogous heme-thiolate active site of cytochrome P450, with O−O bond cleavage leading to the highly oxidizing oxo-ferryl (Fe^{V}═O) species (*31*). K48 in SOR could, thus, direct decay of the intermediate toward hydrogen peroxide formation and away from potentially toxic P450-type oxidative chemistry.

Following our initial report (*7*), Lombard et al. reported a pulse radiolysis study on reaction of superoxide with a closely homologous (70% sequence-identical) 2Fe-SOR from *D. baarsii* (*17*), which was interpreted as proceeding via two successive intermediates at pH 7.6 (the only pH reported). The first of these intermediates formed on a time scale similar to that which we observed for formation of the 600-nm intermediate of *D. vulgaris* SOR and had similar absorption features. The second *D. baarsii* 2Fe-SOR intermediate was reported to maximize at ~5-ms reaction time and to show a red-shifted absorption maximum with a significant increase in absorption intensity relative to the first intermediate. The same study reported similar consecutive chromophoric intermediates for an E47A variant of *D. baarsii* 2Fe-SOR. As emphasized above, our results provide no clear evidence for a second distinct chromophoric intermediate in the reactions of either wild-type or E47A *D. vulgaris* 2Fe-SORs with superoxide. If the bracketed species shown in Scheme 2 corresponds to the second intermediate seen in the *D.*

baarsii 2Fe-SOR, it does not accumulate sufficiently to be detected in *D. vulgaris* 2Fe-SOR. Pulse radiolysis of a K48I variant of *D. baarsii* 2Fe-SOR (*17*) gave kinetics and spectral features of two consecutive intermediates that might be more similar to the intermediate and final product we observed for the K48A variant of *D. vulgaris* 2Fe-SOR, but with differing effects on rates. The K48I substitution was reported to slow the formation rate 20−30-fold (vs the 6−7-fold slowing we observed for *D. vulgaris* K48A) but to have no effect on decay rate (vs 3−4-fold slowing for the *D. vulgaris* K48A). A second pulse radiolysis study by the same group on a 1Fe-SOR from *T. pallidum* also reported two consecutive chromophoric intermediates, with spectral features similar to those reported for the *D. baarsii* 2Fe-SOR (*16*). Pulse radiolysis kinetics of a 1Fe-SOR from *Archaeoglobus fulgidus* (*18*), which were measured in the same laboratory used for our studies, detected only a single intermediate. The rate of formation and spectral properties of the *A. fulgidus* 1Fe-SOR intermediate closely resembled the 600-nm species that we observed for the *D. vulgaris* 2Fe-SOR, but decayed to the "resting" oxidized form ~250-times faster. Even if it were turnover-limiting, the much slower decay rate constant for *D. vulgaris* 2Fe-SOR is likely to be orders of magnitude faster than spontaneous disproportionation of superoxide in vivo.[3]

In fact, none of the pulse radiolysis studies published to date directly address SOR turnover. The exogenous electron donor(s) that would return the ferric $[Fe(NHis)_4(SCys)]$ site to the ferrous form (and perhaps also reduce the $[Fe^{III}(SCys)_4]$ site) in vivo has (have) not been identified. Coulter and Kurtz (*14*) recently showed that *D. vulgaris* rubredoxin catalyzes reduction of both iron sites in *D. vulgaris* 2Fe-SOR and serves as a catalytically competent proximal electron donor to 2Fe-SOR in a newly developed SOR turnover assay. The catalytic turnover mechanism as well as the role of the $[Fe(SCys)_4]$ site in 2Fe-SOR are subjects of continuing investigations in our laboratories.

ACKNOWLEDGMENT

We thank Radu Silaghi-Dumitrescu for helpful discussions.

SUPPORTING INFORMATION AVAILABLE

Tables listing formate and Tris concentration dependencies of the 600-nm intermediate formation and decay rates, ionic strength dependence of formation and decay rates of the intermediate for K48A SOR, Erying plot from which activation parameters were derived, absorption spectra of the 600-nm intermediate and final product generated using 0.5 M ethanol in place of formate, and absorbance vs time traces and scanning spectrophotometry for stopped-flow monitoring of SOR_{pink} oxidations by ferricyanide. This material is available free of charge via the Internet at http://pubs.acs.org.

[3] At pH 7 and 25 °C, the 600-nm intermediate decays with a first-order rate constant of 270 s^{-1} (cf. Table 1). Under the same conditions, superoxide disproportionates with a second-order rate constant of $\sim 5 \times 10^5$ M^{-1} s^{-1}(*26*). Thus, in order for spontaneous disproportionation to compete with decay of the 600-nm intermediate, the intracellular steady-state superoxide concentration would have to be $\sim 10^{-3}$ M, which is probably several orders of magnitude above the lethal level. While no estimates are available for sulfate-reducing bacteria, in aerobically growing *E. coli*, the steady-state intracellular superoxide concentration is estimated to be 10^{-10} M, and to be just below the threshold of lethality (*32*).

REFERENCES

1. Pianzzola, M. J., Soubes, M., and Touati, D. (1996) *J. Bacteriol. 178*, 6736−6742.
2. Liochev, S. I., and Fridovich, I. (1997) *J. Biol. Chem. 272*, 25573−25575.
3. Jenney, F. E., Jr., Verhagen, M. F. J. M., Cui, X., and Adams, M. W. W. (1999) *Science 286*, 306−309.
4. Lumppio, H. L., Shenvi, N. V., Summers, A. O., Voordouw, G., and Kurtz, D. M., Jr. (2001) *J. Bacteriol. 183*, 101−108.
5. Yeh, A. P., Hu, Y., Jenney, F. E., Jr., Adams, M. W., and Rees, D. C. (2000) *Biochemistry 39*, 2499−2508.
6. Coehlo, A. V., Matias, P., Fülop, V., Thomson, A., Gonzalez, A., and Carrondo, M. A. (1997) *J. Biol. Inorg. Chem. 2*, 680−689.
7. Coulter, E. D., Emerson, J. P., Kurtz, D. M., Jr., and Cabelli, D. E. (2000) *J. Am. Chem. Soc. 122*, 11555−11556.
8. Brumlik, M. J., and Voordouw, G. (1989) *J. Bacteriol. 171*, 4996−5004.
9. Moura, I., Tavares, P., Moura, J. J., Ravi, N., Huynh, B. H., Liu, M. Y., and LeGall, J. (1990) *J. Biol. Chem. 265*, 21596−21602.
10. Tavares, P., Ravi, N., Moura, J. J. G., LeGall, J., Huang, Y.-H., Crouse, B. R., Johnson, M. K., Huynh, B. H., and Moura, I. (1994) *J. Biol. Chem. 269*, 10504−10510.
11. Lombard, M., Fontecave, M., Touati, D., and Niviere, V. (2000) *J. Biol. Chem. 275*, 115−121.
12. Clay, M. D., Jenney, F. E., Jr., Hagedoorn, P. L., George, G. N., Adams, M. W. W., and Johnson, M. K. (2001) *J. Am. Chem. Soc. ASAP article*.
13. Verhagen, M. F. J. M., Voorhorst, W. G., Kolkman, J. A., Wolbert, R. B., and Hagen, W. R. (1993) *FEBS Lett. 336*, 13−18.
14. Coulter, E. D., and Kurtz, D. M., Jr. (2001) *Arch. Biochem. Biophys. 394*, 76−86.
15. Romao, C. V., Liu, M. Y., Le Gall, J., Gomes, C. M., Braga, V., Pacheco, I., Xavier, A. V., and Teixeira, M. (1999) *Eur. J. Biochem. 261*, 438−443.
16. Niviere, V., Lombard, M., Fontecave, M., and Houee-Levin, C. (2001) *FEBS Lett. 497*, 171−173.
17. Lombard, M., Houee-Levin, C., Touati, D., Fontecave, M., and Niviere, V. (2001) *Biochemistry 40*, 5032−5040.
18. Abreu, I. A., Saraiva, L. M., Soares, C. M., Teixeira, M., and Cabelli, D. E. (2001) *J. Biol. Chem. 276*, 38995-39001.
19. Carlioz, A., and Touati, D. (1986) *EMBO J. 5*, 623−630.
20. Schagger, H., and von Jagow, G. (1987) *Anal. Biochem. 166*, 368−379.
21. McCord, J. M., and Fridovich, I. (1969) *J. Biol. Chem. 244*, 6049−6055.
22. Coulter, E. D., Shenvi, N. V., and Kurtz, D. M., Jr. (1999) *Biochem. Biophys. Res. Commun. 255*, 317−323.
23. Goto, J. J., Gralla, E. B., Valentine, J. S., and Cabelli, D. E. (1998) *J. Biol. Chem. 273*, 30104−30109.
24. Schwarz, H. A. (1981) *J. Chem. Educ. 58*, 101−105.
25. Abreu, I. A., Saraiva, L. M., Carita, J., Huber, H., Stetter, K. O., Cabelli, D., and Teixeira, M. (2000) *Mol. Microbiol. 38*, 322−334.
26. Bielski, B. H. J., and Cabelli, D. (1991) *Int. J. Radiat. Biol. 59*, 291−319.
27. Apiyo, D., Jones, K., Guidry, J., and Wittung-Stafshede, P. (2001) *Biochemistry 40*, 4940−4948.
28. Xiong, J., Phillips, R. S., Kurtz, D. M., Jr., Jin, S., Ai, J., and Sanders-Loehr, J. (2000) *Biochemistry 39*, 8526−8536.
29. Farmer, C. S., Kurtz, D. M., Jr., Phillips, R. S., Ai, J., and Sanders-Loehr, J. (2000) *J. Biol. Chem. 275*, 17043−17050.
30. Williams, A., and Frasca, V. (1999) in *Current Protocols in Protein Science* (Coligan, J. E., Dunn, B. M., Ploegh, H. L., Speicher, D. W., and Wingfield, P. T., Eds.) pp 8.2.1−8.2.30, John Wiley & Sons, Inc., New York.
31. Loew, G. H., and Harris, D. L. (1998) *J. Am. Chem. Soc. 120*, 8941−8948.
32. Gort, A. S., and Imlay, J. A. (1998) *J. Bacteriol. 180*, 1402−1410.

BI0119159